TU Delft

Delft University of Technology

An Innovative Visual Weighing Method
Measuring Bulk Material Mass Flows via Belt Deformation Field With Deep Learning

Qiao, Wei; Xiong, Xiaoyan; Jie, Chen; Dong, Huijie; Pang, Yusong; Yu, Junzhi

DOI
10.1109/TII.2024.3470897

Publication date
2025

Document Version
Final published version

Published in
IEEE Transactions on Industrial Informatics

Citation (APA)
Qiao, W., Xiong, X., Jie, C., Dong, H., Pang, Y., & Yu, J. (2025). An Innovative Visual Weighing Method: Measuring Bulk Material Mass Flows via Belt Deformation Field With Deep Learning. *IEEE Transactions on Industrial Informatics*, *21*(1), 960-969. https://doi.org/10.1109/TII.2024.3470897

Important note
To cite this publication, please use the final published version (if applicable).
Please check the document version above.

Copyright
Other than for strictly personal use, it is not permitted to download, forward or distribute the text or part of it, without the consent of the author(s) and/or copyright holder(s), unless the work is under an open content license such as Creative Commons.

Takedown policy
Please contact us and provide details if you believe this document breaches copyrights.
We will remove access to the work immediately and investigate your claim.

This work is downloaded from Delft University of Technology.
For technical reasons the number of authors shown on this cover page is limited to a maximum of 10.

Green Open Access added to TU Delft Institutional Repository

'You share, we take care!' - Taverne project

https://www.openaccess.nl/en/you-share-we-take-care

Otherwise as indicated in the copyright section: the publisher is the copyright holder of this work and the author uses the Dutch legislation to make this work public.

An Innovative Visual Weighing Method: Measuring Bulk Material Mass Flows via Belt Deformation Field With Deep Learning

Wei Qiao, Xiaoyan Xiong, Chen Jie, Huijie Dong, *Member, IEEE*, Yusong Pang, and Junzhi Yu, *Fellow, IEEE*

***Abstract*—This article presents an innovative visual method for measuring material mass online by quantified conveyor belt deformation with deep learning, which offers a noncontact and safe alternative to traditional pressure- and radioactivity-based weighing techniques. The correlation between the belt deformation and the carried material mass is further investigated through finite element simulations. Then, a visual weighing method by belt deformation is proposed, comprising a calibration algorithm to construct a measurement model using a gated recurrent unit-based network, and an online measurement algorithm to calculate material mass with the trained network. Finally, a case study is presented to analyze the effect of different dimension configurations and networks. The results validate that the proposed method attains a notable accuracy and is suitable for high-velocity conveyor environments. The demonstrated benefits signify an advancement in visual perception of materials, enabling a new approach for intelligent operation and monitoring in material handling field.**

***Index Terms*—Belt conveyor, belt deformation, deep learning, gated recurrent unit (GRU), mass estimation, material mass flow measurement.**

Received 8 June 2024; revised 1 September 2024; accepted 24 September 2024. Date of publication 14 October 2024; date of current version 7 January 2025. This work was supported in part by the Science and Technology Major Project of Inner Mongolia under Grant 2021ZD0004 and in part by the Patent Conversion Special Plan of Shanxi Province under Grant 202305005. Paper no. TII-24-2864. *(Corresponding author: Xiaoyan Xiong.)*

Wei Qiao and Xiaoyan Xiong are with the College of Mechanical and Vehicle Engineering, Taiyuan University of Technology, Taiyuan 030024, China, and also with the Key Laboratory of Advanced Transducers and Intelligent Control System, Ministry of Education, Taiyuan University of Technology, Taiyuan 030024, China (e-mail: qiaowei0016@link.tyut.edu.cn; xiongxiaoyan@tyut.edu.cn).

Chen Jie and Huijie Dong are with the Key Laboratory of Advanced Transducers and Intelligent Control System, Ministry of Education, Taiyuan University of Technology, Taiyuan 030024, China (e-mail: jiechen0231@link.tyut.edu.cn; donghuijie@tyut.edu.cn).

Yusong Pang is with the Section of Transportation Engineering and Logistics, Department of Maritime and Transport Technology, Delft University of Technology, 2628CD Delft, The Netherlands (e-mail: y.pang@tudelft.nl).

Junzhi Yu is with the State Key Laboratory for Turbulence and Complex Systems, Department of Advanced Manufacturing and Robotics, BIC-ESAT, College of Engineering, Peking University, Beijing 100871, China (e-mail: junzhi.yu@ia.ac.cn).

Digital Object Identifier 10.1109/TII.2024.3470897

I. Introduction

BELT conveyors are essential for transporting bulk materials and are widely used in mining, ports, power plants, metallurgical plants, and construction sites to enhance efficiency and automation. Measuring the weight of material flow on a conveyor belt is vital for ensuring operational efficiency, quality control, cost management, and safety. The weighing method for conveyor belts involves measuring the weight of bulk materials as they are transported on a moving conveyor belt to provide continuous weight measurements without interrupting the material flow. The real-time weighing of material flows contributes to the reliability and safety of conveyor systems and is indispensable for fault monitoring and implementing energy-saving control schemes [1], [2] in industrial informatics.

Currently, real-time methods for real-time weighing material flows can be categorized into pressure-based methods [3], [4] and radioactivity-based methods [5], [6]. The primary equipment employed in the former approach is an electronic belt scale, which is typically installed beneath a roller. As materials pass through the roller, they exert pressure on it, enabling the mass flow to be calculated by measuring the pressure. However, this contact-based measurement method requires extensive maintenance efforts and is susceptible to factors such as belt tension and vibration. Radioactivity-based weighing is currently the sole noncontact method employed for weighing, wherein the mass of a material is determined by evaluating the degrees of γ-ray penetration and attenuation. However, the use of radioactive substances poses significant security risks, and radioactive sources naturally decay over time. Moreover, the accuracy of this approach can be compromised when materials with markedly different densities are present. The development of a new noncontact and safe detection mechanism is an important research direction for belt weighing.

Different with the aforementioned weighing methods, there is an emerging type of material flow measurement method that involves the direct measurement of the dynamic volume of the target material. These methods are known as volumetric flow measurement methods. Common volumetric flow measurement methods include ultrasonic, laser [7], [8], and machine vision [9], [10], [11], [12] approaches. In these methods, the mass flow is calculated based on the measured material volume, the empirical stacking rate, and the average material density. Thus, the approach of weighing by volumetric flow measurement directly correlates volume and mass, while introducing personal error through the determination of the empirical stacking rate and the average material density. With the rapid development of

1941-0050 © 2024 IEEE. Personal use is permitted, but republication/redistribution requires IEEE permission.
See https://www.ieee.org/publications/rights/index.html for more information.

Authorized licensed use limited to: TU Delft Library. Downloaded on January 27,2025 at 09:33:04 UTC from IEEE Xplore. Restrictions apply.

vision acquisition technology and artificial intelligence theory, research on intelligent visual perception has become a focal point in the field of industrial intelligence [13]. Direct measurement of material mass through visual methods, rather than volume, represents an innovative weighing approach. Such approach can offer seamless integration with various inspection parameters on belt conveyors, including belt deviation, longitudinal tearing, material volume, and distribution patterns, to form a comprehensive visual monitoring system. By doing so, it provides richer operational state information, enhancing monitoring and decision-making capabilities. It can promote the development of cyber-physical systems in material handling field. To realize this weighing method effectively, it is crucial to establish a correlation between visual observations and material mass.

The mass of materials cannot be directly determined visually, necessitating the utilization of an observable characteristic associated with weight. When loading materials, a conveyor belt experiences deformation and sagging due to its inherent resilience. This phenomenon is influenced by various factors, including the mass and distribution of the materials and the belt tension. However, the trough shape of the conveyor belt, along with its viscoelastic properties and material distribution uncertainties, poses challenges in terms of directly characterizing the relationships between the overall deformation and other influencing factors using mathematical formulas. Dynamic simulation methods, such as the finite element method (FEM) and the discrete element method (DEM), have been widely employed by researchers to analyze belt sag in conveyor belts due to their ability to overcome the limitations of static methods [14]. Ilic et al. [15] utilized the DEM to measure and simulate the loads acting on a conveyor belt during the transportation process in cases with various solid bulk materials and different belt sag ratios. Shen et al. [16], [17] proposed numerical methods that couple the FEM and DEM for dynamic belt deflection prediction. Bolat et al. [18] investigated the effects of different conveyor angles on conveyor capacities and belt sags using the FEM and DEM. These studies have collectively demonstrated the substantial impact of material quantity on belt deformation. However, they focused primarily on the monodirectional influences of materials on belt deformation and lacked numerical models for online calculations of the masses of materials from belt deformations. It is a potential solution to model the corresponding correlation between belt deformation and material mass for real-time weighing. The primary challenge in such a solution lies in establishing a measurement model that captures the inherent correlation between belt deformation and material mass, enabling real-time measurements.

This article presents an innovative visual weighing method for measuring material mass by quantified belt deformation and a deep learning (DL) algorithm, in which a weighing principle by belt deformation is, to the best of our knowledge, implemented and validated for the first time internationally. This research makes the following main three contributions.

1) The correlation between the belt deformation and the carried material mass is further investigated through an FEM simulation. The concepts of the belt deformation field and the deformation matrix are defined, in which the former serves as a standardized mathematical representation of the belt deformation while the latter represents a discretized sample of the former.
2) An innovative online visual weighing method by belt deformation is proposed. A measurement scheme is designed based on the FEM analysis. Then, a calibration method is proposed to construct a measurement model to calculate corresponding material mass by a specific belt deformation matrix. Due to the complexity of the model, a gated recurrent unit (GRU)-based network is designed to serve as the measurement model by regression training. Subsequently, an online measurement method is presented to calculate total material mass using the trained measurement model.
3) Systematic experimentation and comparison with other common DL networks are performed in a case study. Several datasets have been constructed for deformation matrices with different dimensions, and suitable dimension configurations are determined based on the experimental results to give a value reference for the practical employment of the proposed measurement method. The results also validate the feasible and effectiveness of our proposed measurement method.

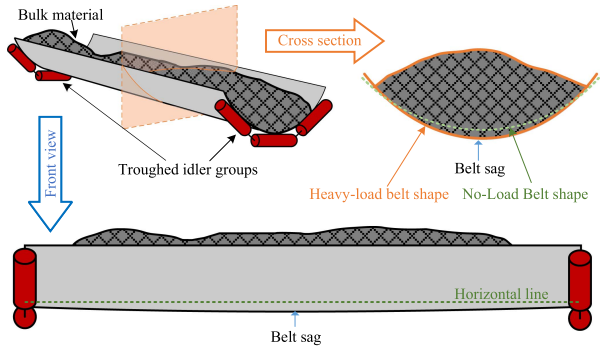

Fig. 1. Deformation and sag of a conveyor belt within the idler spacing.

The compatibility between the proposed method and volume measurement method also stands out, facilitating simultaneous mass and volume flow monitoring within a unified system, which provides technical support for improving online monitoring capabilities in the field of material handling and for digital twin applications in material handling.

The rest of this article is organized as follows. Section II analyzes the relationship between the material load and belt deformation by FEM simulations. Section III illustrates the concepts of the belt deformation field and deformation matrix. The measurement method including calibration and online measurement is described in Section IV. Section V presents the case study and experimental verification. Finally, Section VI concludes this article.

II. Belt Deformation Analysis

When loading materials, a conveyor belt experiences deformation, which is a visually observable characteristic directly caused by the mass of the materials. Belt sag occurs within the idler spacing, which refers to the distance between two consecutive idlers of the conveyor. As illustrated in Fig. 1, in areas lacking support from idler sets, the distribution of materials influences the deformation trend of the belt. However, it is difficult to measure the deformation on the whole belt surface in real time. It is essential to quantitatively analyze the influence of material mass and distribution on belt deformation for the determination of a vision-based weighing scheme.

Authorized licensed use limited to: TU Delft Library. Downloaded on January 27,2025 at 09:33:04 UTC from IEEE Xplore. Restrictions apply.

TABLE I
SPECIFICATIONS OF THE BELT CONVEYOR APPLIED IN THE FINITE ELEMENT SIMULATIONS

Description	Value	Description	Value
Idler trough angle	20°	Belt thickness	12 mm
Belt width	800 mm	Idler roll length	280 mm
Elasticity modulus	64.9 N/mm^2	Poisson's ratio	0.28
Density	1365 kg/m^3	Idler spacing	880 mm

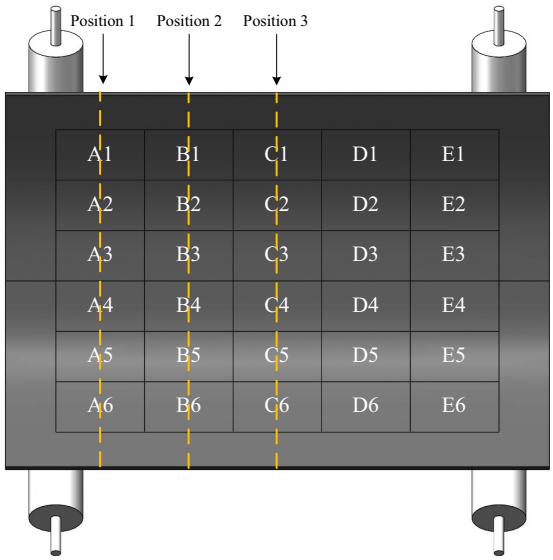

Fig. 2. Segmentation of the material loading zones in the finite-element simulations.

To systematically examine the deformation responses of conveyor belts under material-induced loads, finite element simulations are employed to elucidate their interactions. The parameters characterizing the employed conveyor belt are presented in detail in Table I. While the velocity of the belt may affect its interaction with the conveyed bulk material, its influence on the dynamic deformation process of the belt is considered negligible for the purpose of this analysis [17]. Consequently, the simulations are restricted to a static scenario within the idler spacing to facilitate a focused analysis.

The loading region of the belt is segmented into 30 discrete zones (A1–E6) to model the distribution of the load, as illustrated in Fig. 2. To effectively capture the deformation characteristics, detection points are strategically located along the central longitudinal axes of zones A, B, and C.

Preliminary finite element simulations are performed to explore the conveyor belt deformation induced by uniformly distributed loads at A3A4, B3B4, and C3C4. The resultant deformation profiles are delineated in Fig. 3, which distinctly illustrates the augmented effect of centrally positioned loads on the deformation process of the belt.

Furthermore, the contour curves corresponding to the three detection positions are exhibited in Fig. 4. From the simulation results, we can infer the following: 1) the deformation trend is more pronounced directly beneath the applied loads, underscoring the localized influence of material weight; 2) the presence of materials affects the deformation pattern of the belt even in adjacent sections that are not in immediate contact with the load;

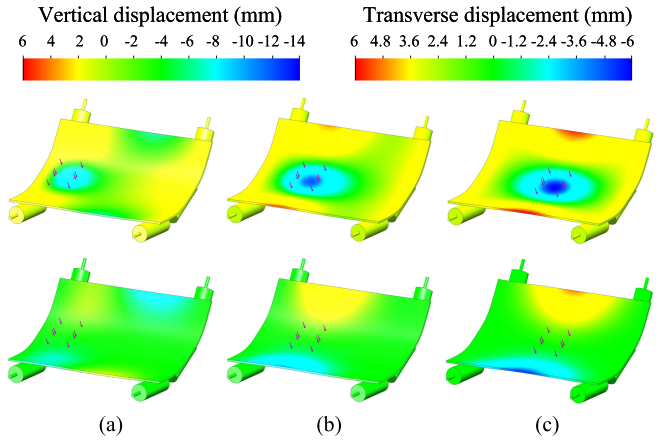

Fig. 3. Deformation profiles produced by loads on different area. (a) Loads are situated at A3A4. (b) Loads are situated at B3B4. (c) Loads are situated at C3C4.

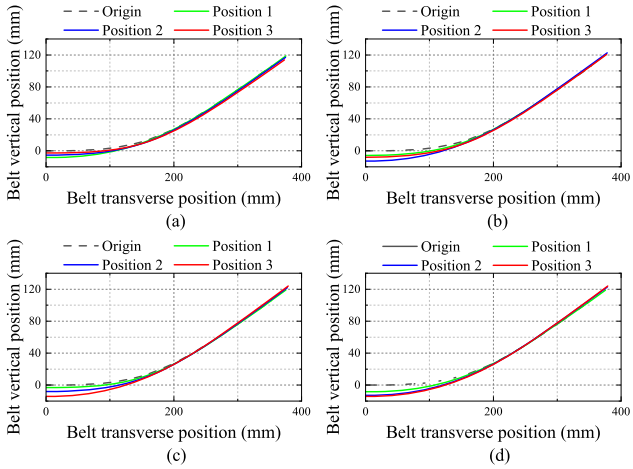

Fig. 4. Belt contour curves corresponding to the three detection positions. (a) Loads situated at A3A4. (b) Loads situated at B3B4. (c) Loads situated at C3C4. (d) Loads situated at corresponding detection zones.

3) central loading zones are subjected to greater degrees of deformation than other areas are, indicating the significant sensitivity of the midsection of the belt to load-induced distortions.

The responses of the conveyor belt to various loads and their distributions are meticulously evaluated, and the results are systematically compiled in Fig. 5. For clarity, a notational system is employed, e.g., "200C3C4" signifies a load of 200 N uniformly allocated across zones C3 and C4; analogous nomenclature is adopted for other loading scenarios.

Fig. 5(a) presents the transverse deformations of the belt under heterogeneous load distributions with an invariant aggregate load. The belt contours vary with the load distributions. Fig. 5(b) illustrates how the deformation patterns vary with a shift in the distribution of a constant total load. The belt deformation trend is contingent on the load distribution under a fixed total load, resulting in deformation nonuniformity. In the scenarios depicted in Fig. 5(c), the load distributions are similar when the total load is modulated, leading to observable disparities in the resulting deformations. Intriguingly, in Fig. 5(d), despite variations in both the magnitudes and distribution patterns of the loads, the resulting deformation curves display remarkable

Authorized licensed use limited to: TU Delft Library. Downloaded on January 27,2025 at 09:33:04 UTC from IEEE Xplore. Restrictions apply.

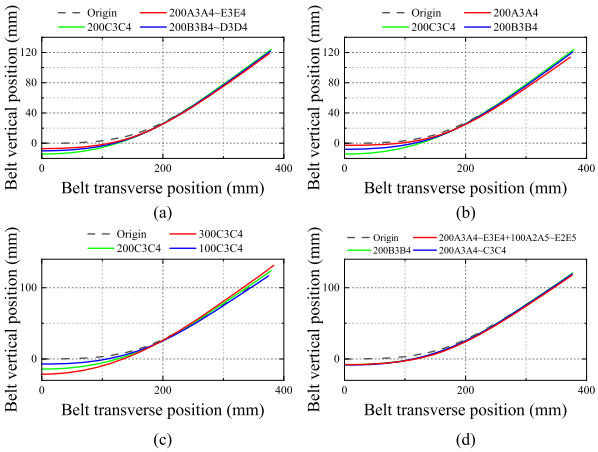

Fig. 5. Transverse belt deformation induced under heterogeneous load distributions. (a) The cases of heterogeneous load distributions with a constant total load. (b) The cases of shifted load application area with a constant total load. (c) The cases of different total load exerted on the same area. (d) Some cases resulting in comparable deformation patterns despite varying load conditions.

resemblance, suggesting a complex interplay between the load parameters and belt deformation.

The above observation indicates that the conveyor belt at the midpoint of the idler spacing is most sensitive to deformation due to the material load. However, inferring the material mass solely from the contour at the midpoint is unreasonable, as different material masses with specific distributions can produce very similar deformation profiles at this position. Limited detection accuracy in practice can lead to these curves being indistinguishable, making it difficult to obtain a mapping from the deformation curve to the material mass. Thus, it is necessary to construct a variable that reflects the conveyor belt deformation, which is significantly correlated with the material mass and has a mapping relationship with it.

III. Belt Deformation Variable Definition

A. Belt Deformation Field

For numerical description of belt deformation, we introduce a scalar field concept called the conveyor belt deformation field to characterize the vertical deflection of each point on the conveyor belt. As shown in Fig. 6(a), each point on a contour line of the conveyor belt theoretically corresponds to a point after deformation, and this transformation relationship correlates with the load. However, in practical detection, it is only possible to obtain the contour curves before and after deformation, without the ability to determine the point-to-point correspondence between the predeformation and postdeformation states, as illustrated in Fig. 6(b).

Therefore, we define the deformation field of the conveyor belt as $h(x, z) = y$, which represents the height of a belt point mapped onto the xoz plane at coordinates (x, z). Assuming that the deformation field when unloaded is $h_0(x, z)$ and the deformation field when loaded is $h_1(x, z)$, $h_1(x, z) - h_0(x, z)$ represents the vertical deflection at each point. Clearly, within the idler space, there is a corresponding relationship between the deformation field and the material distribution.

Considering the real-time requirements, capturing more points in a single measurement consumes more computational

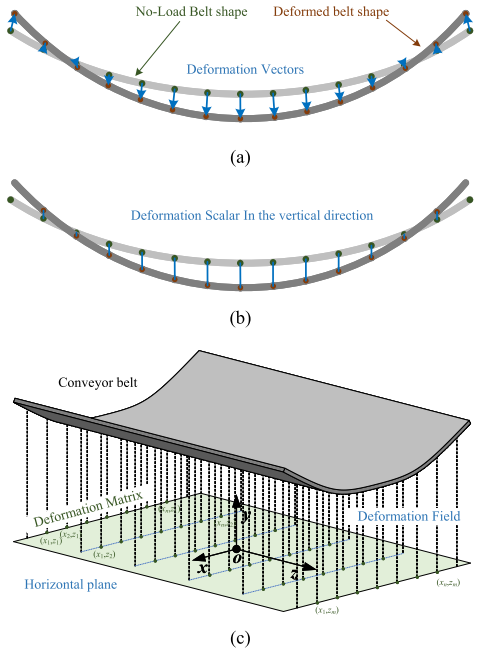

Fig. 6. Schematic diagram of the conveyor belt deformation field. (a) Theoretical deformation vector. (b) Detectable deformation scalar. (c) Defined deformation field represented by height.

resources and time, making real-time measurement infeasible. By balancing the number of measurement points with the real-time requirements, it is commonly used to capture the contour line of the conveyor belt at a cross-section in a single measurement for continuously moving conveyor belts. Thus, the deformation measurement is conducted on a single cross-section, capturing only the conveyor belt contour at the measurement plane. For such situation, we further define a modified deformation field to $h'(x, z) = y'$, in which y' represents the height of the belt point (x, z) as it passes through the measurement plane.

B. Deformation Matrix

In general, high-dimensional input features can make it difficult for a measurement model to calculate measured amount. Therefore, the deformation field needs to be discretized for subsequent calculation. We define the deformation matrix D, which represents the deformation field sampled at rectangular scatter points

$$D = \begin{bmatrix} h'(x_1, z_1) & h'(x_2, z_1) & \dots & h'(x_n, z_1) \\ h'(x_1, z_2) & h'(x_2, z_2) & \dots & h'(x_n, z_2) \\ \vdots & \vdots & \ddots & \vdots \\ h'(x_1, z_m) & h'(x_2, z_m) & \dots & h'(x_n, z_m) \end{bmatrix} \quad (1)$$

where m is the number of rows, which indicates the number of sampled cross-sections, and n is the number of columns, which represents the number of sampled points on each cross-section. Each row in the matrix is obtained from a single measurement. Thus, for each deformation matrix calculated after acquiring a real-time contour, the first row is derived from the current contour line, while the others are historical data. Consequently, this matrix can represent the deformation from cross-sections $z = z_1$ to $z = z_m$ on the conveyor belt.

Authorized licensed use limited to: TU Delft Library. Downloaded on January 27,2025 at 09:33:04 UTC from IEEE Xplore. Restrictions apply.

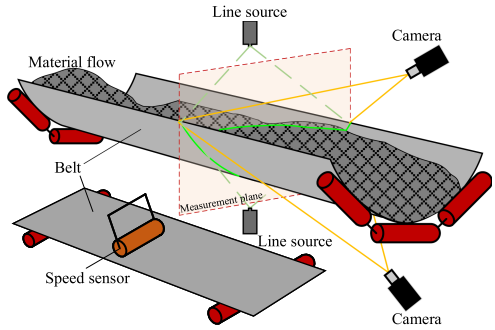

Fig. 7. Noncontact weighing scheme for material mass on conveyor belt.

IV. Visual Weighing Method by Belt Deformation

A. Measurement Scheme

Following the analysis of belt deformation in Section II, we develop a measurement scheme on the basis of a dual-field material volume flow detection method described in [19]. This scheme detects both the contours of the conveyor belt and the materials at the center cross section of the idler spacing, as shown in Fig. 7. The scheme employs two line laser sources to generate contour lines on the material and belt surface, which are then captured in real time by a pair of cameras. In addition, a standard speed sensor is used to monitor the belt speed.

Importantly, only the lower camera is used to detect the conveyor belt deformation. The upper camera captures material distribution information, which is essential for calibrating the relationship between the material mass and belt deformation.

B. Calibration Method

As belt scales require calibration during initial installation to establish the relationship between pressure and material mass, the method of measuring material mass through belt deformation also necessitates a calibration process. This calibration aims to determine the measurement model, which is the mapping relationship from the deformation matrix to its corresponding material mass. Therefore, quantitative experiments are necessary to obtain data.

A single experiment for calibration is as shown in Fig. 8(b). A known mass of material is placed in the loading area, and then the conveyor belt is operated at a constant speed while recording a stream of images as the loading area passes through the idler space. The two cameras employ hardware-synchronized triggering to simultaneously capture comprehensive video footage. The video recording the material profile from the upper camera is denoted as VM, while the video capturing the belt profile from the lower camera is designated as VB. Through multiple experiments with varying total masses and distributions, a set of video pairs $\{(\mathrm{VM}_k, \mathrm{VB}_k)\}$ is obtained. The total material mass in the kth experiment is represented by Q_k. The belt speed is defined as v_b and the frame rate of cameras is defined as f, so that the frame-to-frame distance $d_f = v_b/f$.

In a single experiment, only the total mass is known, whereas the calibration requires segmented mass value corresponding to the region of the deformation matrix. Placing material solely in the region of deformation matrix would significantly increase the number of required experiments, rendering the calibration process exceptionally time-consuming. Therefore, we obtain

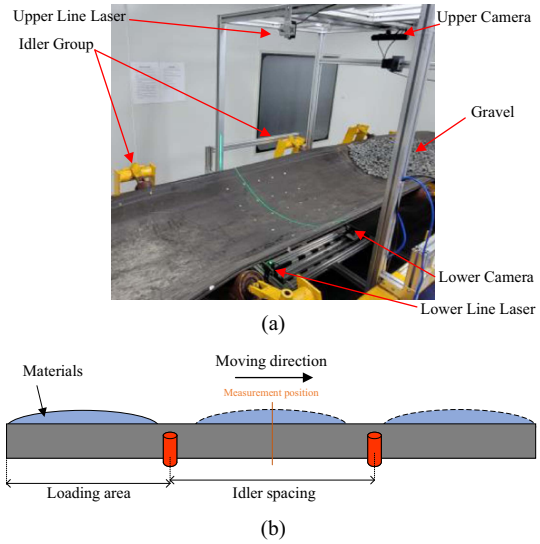

Fig. 8. Experimental scheme for calibrating the measurement model. (a) Actual measurement system. (b) Process of a single experiment for calibration.

segmented mass value through calculations of the material distribution to achieve data upsampling. Assuming that the material used is homogeneous and relatively uniform, the required segmented mass can be obtained by multiplying the proportion of the segment's volume to the total volume by the total mass.

The proposed calibration algorithm is presented in Algorithm 1. The first step involves processing each video pair $(\mathrm{VM}_k, \mathrm{VB}_k)$ frame by frame to obtain the actual coordinate sets $A(i) = \{(x_m, y_m, id_f)\}$ representing the material profile and $B(i) = \{(x_b, y_b, id_f)\}$ representing the belt profile, where $i = 1, 2, \ldots n_p$ denotes the frame number, and $z = id_f$ corresponds to the cross-sectional position of that frame. The image processing aims to extract the laser line contour and convert it to world coordinates based on the camera's intrinsic and extrinsic parameters. This process has been extensively studied [19] and will not be elaborated upon in this article. Subsequently, the area enclosed by the two curves represented by $A(i)$ and $B(i)$ is calculated, yielding the material cross-sectional area $S(i)$ for that frame. Multiplying by d_f gives the material volume for that frame, $V(i) = d_f S(i)$. After completing calculations for all frames in the video, the deformation field $h'(x_b, z_b) = y_b$ can be obtained through the union of all $B(i)$, where $z_b \in id_f | i = 1, 2, \ldots, n_p$. The total volume in this trial is calculated by $V_s = \sum V(i)$. The second step involves determining the sampling points $\{(x_s, z_s)\}$ based on m and n, where x_s can be uniformly selected according to the value of n and the actual belt width, and z_s can be set as $z_s = 0, d, \ldots, (m-1)d$. For convenience, d can be set as an integer multiple of d_f, i.e., $d = ld_f$ where $l \in \mathbb{N}$. Starting from the first frame, the deformation matrix is sampled, and the corresponding segmented mass is calculated. The deformation matrix $D(j)$ is calculated using (1) for all points at positions $(x, z) = (x_s, jd_f + z_s)$, with the corresponding segmented mass given by

$$q_j = \frac{Q_k}{V_s} \sum_{i=j}^{j+(m-1)l} V(i) \tag{2}$$

This yields the input-output data pair (D_j, q_j), which is stored in the dataset. The loop process is performed until $j+(m-1)l > n_p$.

Authorized licensed use limited to: TU Delft Library. Downloaded on January 27,2025 at 09:33:04 UTC from IEEE Xplore. Restrictions apply.

Algorithm 1: Calibration algorithm for visual weighing.

for $k = 1, 2, \ldots$ **do**
  Read experimental videos $\mathrm{VM}_k, \mathrm{VB}_k$
  for $i = 1, 2, \ldots, n_p$ **do** ▷Step 1
    Read i-th frame in VM_k
    Perform image processing, obtain coordinate set of material contour $A(i) = \{(x_m, y_m, id_f)\}$
    Read i-th frame in VB_k
    Perform image processing, obtain coordinate set of belt contour $B(i) = \{(x_b, y_b, id_f)\}$
    Calculate cross-sectional area $S(i)$ enclosed by $A(i)$ and $B(i)$
    Calculate single-frame volume $V(i) = d_f S(i)$
  Calculate total volume $V_s = \sum V(i)$
  Construct deformation field $h'(x_b, z_b) = y_b$ by union of all $B(i)$
  Determine sampling points X_s, Z_s by m, n
  for $j = 1, 2, \ldots, n_p - (m-1)l$ **do** ▷Step 2
    Sample deformation matrix D_j by Eq. (1) for all $(x, z) \in \{(x_s, jd_f + z_s) | x_s \in X_s, z_s \in Z_s\}$
    Calculate segmented mass q_j by Eq. (2)
    Store (D_j, q_j) in dataset
Use D as input and q as output in the dataset for network training until completion ▷Step 3

Algorithm 2: Online material mass measurement algorithm.

while Online measurement is performing **do**
  Read current frame from the lower camera ▷Step 1
  Calculate inter-frame conveying distance $d_c = v_k f_k$
  Calculate current cross-sectional position $z_c = z_l + d_c$
  Perform image processing, obtain coordinate set of belt contour $B = \{(x_b, y_b, z_c)\}$
  Sample specific n points in B, obtain vector ${}^{z=z_c}B_s = \{(x_b, y_b) | x_b \in X_s\}$
  Store ${}^{z=z_c}B_s$ in a queue Q_B
  if Measurement time is reached **then** ▷Step 2
    Record current measurement position as $p_k = z_c$
    Read specific n vectors ${}^{z=z_c}B_s$, ${}^{z=z_c-d}B_s$, ..., ${}^{z=z_c-(m-1)d}B_s$ in history Q_B
    Construct deformation matrix D_k with the n vectors by Eq. (1)
    Input D_k into the trained network, output q_k
    $Q_\sigma(k) = Q_\sigma(k-1) + q_k(p_k - p_{k-1})/(md)$

Through the two steps, a substantial amount of data pairs comprising deformation matrices and corresponding material masses can be obtained. The relationship between the two variable is relatively complex, making it challenging to perform regression using traditional data fitting methods. However, the successful application of DL in industrial informatics [20], [21] offers a potential solution. For example, Zhang et al. [22] proposed a dual-branch deep learning model for accurate fault diagnosis under high-noise conditions. Zhang et al. [23] integrated elastic net algorithm and multilayer perceptron to O_2 concentration in an air separation process. Furthermore, the abundance of data from the two steps lays a solid foundation for the application of deep learning techniques. Consequently, in the third step, we employ a deep neural network architecture to satisfy the dual objectives of achieving a high degree of fitting accuracy and enabling real-time detection capabilities. Our designed model architecture is composed of a GRU layer followed by a fully connected layer. Specifically, the network integrates a GRU layer equipped with 64 neurons. The GRUs in this layer use gating mechanisms to control the flow of information. These mechanisms, known as update and reset gates, are instrumental in capturing temporal dependencies within time series data, regardless of the input sequence length [24]. This characteristic is particularly beneficial for handling the dynamics of conveyor belt deformation data, which exhibit long-term temporal relationships due to the continuous movement of the belt and the progression of material loads over time. Following the GRU layer, the network topology includes a fully connected layer that culminates in a single output neuron. The role of this layer is to map the high-dimensional features learned by the GRU layer onto a single continuous value that represents the measured material mass. The network is trained using the constructed dataset until convergence is achieved, then it can serve as the measurement model for online measurement applications.

Several key considerations should be observed during the calibration process as follows.

1) The calibration should be conducted using the actual transport material with similar size.
2) The loading area should be slightly shorter than the idler spacing.
3) The range of total masses should encompass scenarios from empty to full load conditions.
4) For a given material mass, multiple calibration videos can be recorded with altered distributions to enrich the data amount.

C. Online Measurement Method

After obtaining the measurement model represented by a DL network through calibration, it can be applied for online measurement. The online weighing algorithm for material mass is illustrated in Algorithm 2. The process can be divided into two steps.

The first step involves online reading of frames captured by the lower camera, extracting the belt contour, and obtaining the coordinate set of contour points $B = (x_b, y_b, z_c)$. Here, z_c represents the cross-sectional position captured by current frame, determined by the current belt speed v_k, frame rate f_k, and the position of the previous frame z_l: $z_c = z_l + v_k/f_k$. The specific n points are extracted according to the deformation matrix, forming the vector ${}^{z=z_c}B_s = (x_b, y_b) | x_b \in X_s$, which is then stored in the queue Q_B. The left superscript indicates the cross-sectional position of this vector. This step is executed cyclically at the camera's frame rate.

The second step is only performed when a measurement moment is reached. The current measurement position is recorded as $p_k = z_c$, where k is the current measurement instance. From the queue Q_B, ${}^{z=z_c}B_s$, ${}^{z=z_c-d}B_s$,..., ${}^{z=z_c-(m-1)d}B_s$ are read, and the deformation matrix D_k is constructed. D_k is input into the trained network obtained through calibration, calculating the corresponding segmented mass q_k. Since q_k corresponds to the region represented by D_k, it is converted to the detection area and accumulated. Then, the total material mass measured up to the current moment can be calculated as $Q_\sigma(k) = \sum q_k(p_k - p_{k-1})/(md)$.

Authorized licensed use limited to: TU Delft Library. Downloaded on January 27,2025 at 09:33:04 UTC from IEEE Xplore. Restrictions apply.

V. Case Study

In the proposed measurement method, the optimal dimensions of the deformation matrix need to be determined based on the actual parameters and operational conditions of the belt conveyor. This study conducts tests of the proposed measurement method on an experimental belt conveyor and compares deformation matrices of various dimensions to analyze what kind of dimension configurations is better. First, calibration tests are performed, comparing the application results of multiple DL methods. Subsequently, measurement experiments are conducted using the calibrated network to validate the measurement accuracy. Furthermore, the real-time performance of the measurement system is also evaluated.

The actual measurement system is shown in Fig. 8(a). The loading area is 780 mm in length. The conveyed material is gravel with particle sizes between 1 and 2 cm and a density of approximately 2,864 kg/m^3. The total mass of the material varies from 0 to 70 kg. These recordings are made at a frame rate of 60 fps with a resolution of 1280×720 pixels. The belt speed is maintained at approximately 0.12 m/s, resulting in a frame-to-frame conveying distance of 2 mm.

We design various dimensions of the deformation matrix and construct a dataset for each dimension. Considering that the longitudinal deformation of the belt is relatively smooth, cross-sections are sampled at intervals of $d = 80$ mm. For each cross-section, points are selected at intervals of 10 mm within the range $x \in [-300, 300]$ mm, resulting in 61 points. Under the constraints $m \leq 11$ and $n \leq 61$, the following configurations are chosen: $m \in \{4, 6, 8, 11\}$ and $n \in \{1, 7, 13, 31, 61\}$. When $n = 1$, the point at $x = 0$ is chosen. When $n \neq 1$, points are selected based on equal division, and the set of points is given by

$$x \in \left\{ 10 \left\lfloor \frac{60i}{n-1} \right\rfloor - 300 \middle| i = 0, 1, \ldots, n-1 \right\}$$
$$z \in \{ z_0 + jd | j = 0, 1, \ldots, m-1 \} \quad (3)$$

where $\lfloor \cdot \rfloor$ denotes the floor function and z_0 is the longitudinal position of the conveyor belt currently in the detection plane. Based on these combinations, datasets with different input dimensions were constructed. A total of 109 experiments were conducted, resulting in 46 340 samples for each dataset by Algorithm 1.

A. Calibration Results

In this part, the GRU network representing the measurement model is trained using datasets for each of the aforementioned 20 dimensional configurations. For comparison with the designed GRU network, we design several other DL networks capable of solving regression problems, including a fully connected network (FCN), a convolutional neural network (CNN), and a long short-term memory network (LSTM). The FCN is designed with a hidden layer containing 100 nodes. The CNN employs a convolutional layer with 64 nodes and a kernel length of 3. The LSTM network uses a hidden layer with 64 neurons. All these networks are connected to a fully connected layer with 50 nodes and a single-node output layer to ensure consistency with the designed GRU network. Tests are conducted on network training performance, measurement accuracy, and real-time performance.

The training processes of the four networks are executed using the Python programming language and the TensorFlow framework, with the adaptive moment estimation optimizer employed to dynamically tune the learning rates. The mean squared error (MSE) loss function is utilized. Each dataset is split into training and testing sets at an 8:2 ratio. After the training process, each model is evaluated against a test set to ascertain its generalizability. This evaluation is quantified using several statistical indicators, namely, the root mean square error (RMSE), mean absolute error (MAE), and coefficient of determination, which is denoted as R-squared (R^2).

The progression of the loss function during the training phase over 1000 epochs is depicted in Fig. 9. The inset plots in the figure show the loss values during 900 and 1000 iterations. A rapid convergence of the loss values is noted, particularly for configurations where $n \geq 7$, with the convergence process settling at a loss value below 0.05, which indicates that the designed dataset enables all four models to converge through training. Specifically, among the DL models, the loss values for the LSTM and GRU are smaller. However, an oscillatory pattern is observed when n is set to 61 for the GRU, indicating potential overfitting at higher numbers of sampling points.

The final loss also varies with the dimensions of the deformation matrix. The smallest dimensions of the deformation matrix (4,1) results in the highest final loss values across all network training sessions, but the largest dimensions (11,61) does not achieve a smaller final loss compared to the other dimensions; this indicates that more deformation information does not necessarily benefit network training. In addition, when $n = 1$, the final loss decreases as m increases, but when $n = 61$, the final loss increases as m increases. This phenomenon occurs in the training of all four networks. The above results suggest that by reasonably selecting the dimensions (m, n), the final loss can be minimized to achieve better training results.

After completing 1000 training iterations, the performance metrics are assessed on the test data, and the results are illustrated in Fig. 10. The low values of RMSE and MAE indicate that the predicted values of the models are close to the actual values. An R^2 value close to 1 indicates a strong explanatory power of the model for the data. Except for the dimensions (4,1), the RMSE and MAE values increase with increasing m, while the R^2 values do not differ significantly. This finding suggests that by selecting $m = 4$, good training results can be obtained without requiring a larger m. The smallest RMSE and the largest R^2 are observed in the GRU training with dimensions of (4,31), indicating that the designed GRU-based weighing scheme has better training performance than the other methods.

B. Accuracy Test

Additional experimental videos are used to evaluate the accuracy of the trained networks in quantitatively weighing materials. These experimental videos are not used for model training. The quantitative material masses range from 10 to 70 kg, in increments of 5 kg, resulting in a total of 13 experiments. In each experiment, all frames are used to calculate belt deformation field as Algorithm 2. Since the interframe distance is 2 mm and the cross-sectional spacing d of the deformation matrix is set to 80 mm, each total mass is measured 39 times through different deformation matrices in the belt deformation field. The mean and standard deviation of the measurements for each total mass are calculated to determine the measurement accuracy, and the average accuracy of these different masses is taken as the final measurement accuracy.

The final accuracy results are shown in Fig. 11. The results show that different networks achieve the highest accuracy at different (m, n). The FCN achieves its best accuracy of 92.38±2.00% at $(8, 1)$. The CNN achieves its best accuracy

Authorized licensed use limited to: TU Delft Library. Downloaded on January 27,2025 at 09:33:04 UTC from IEEE Xplore. Restrictions apply.

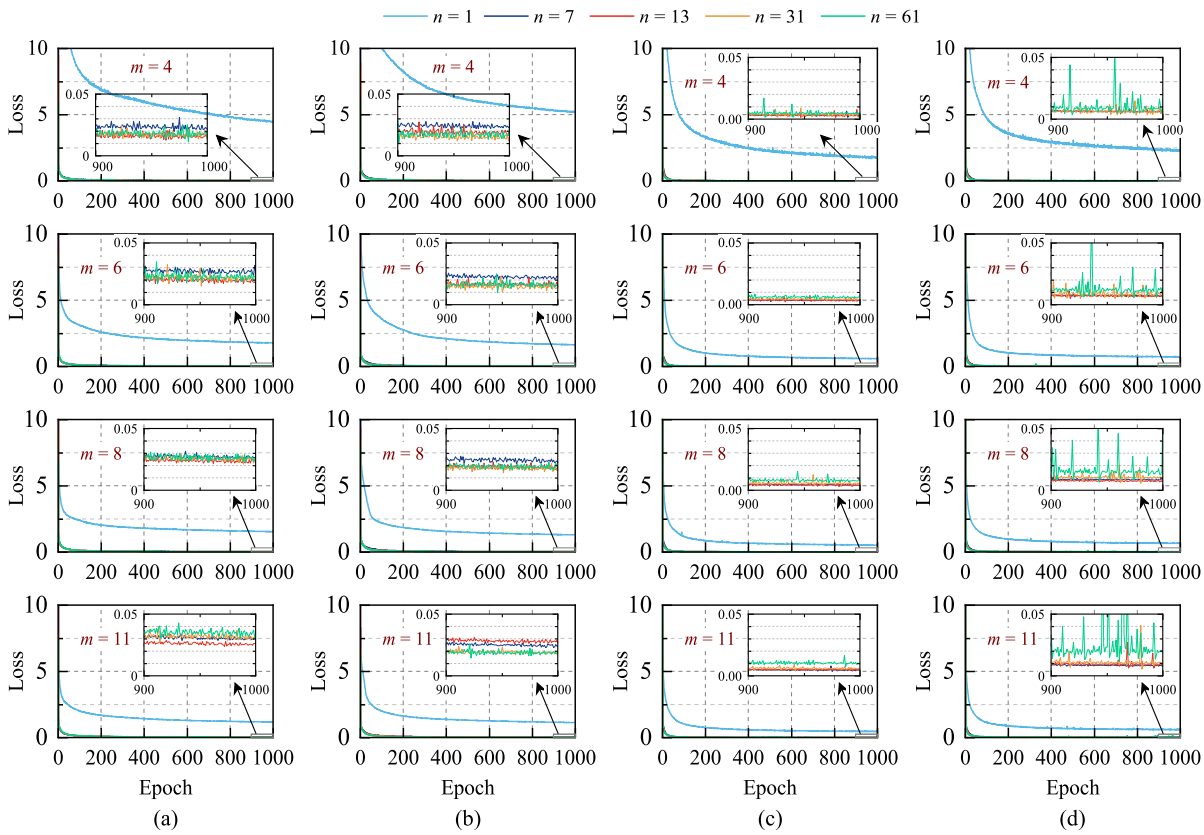

Fig. 9. Progression of the loss function during the training phase under different dimensions (m, n) and different networks. (a) FCN. (b) CNN. (c) LSTM. (d) GRU.

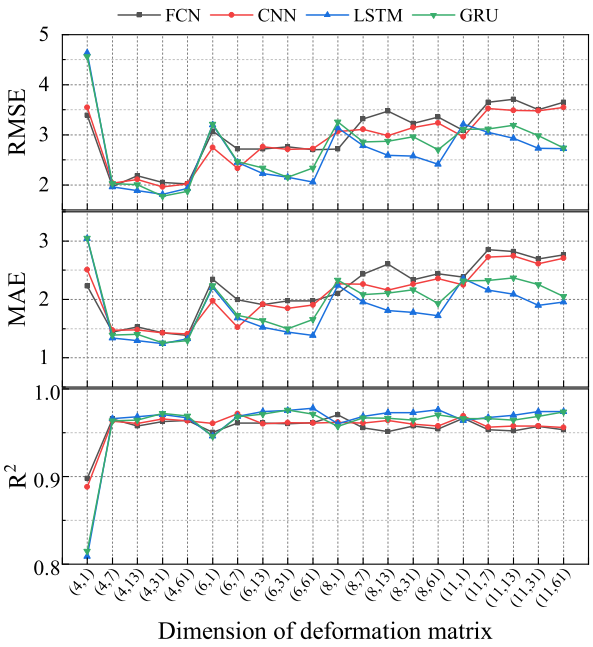

Fig. 10. Performance metrics after completing 1000 training iterations with different deformation matrix dimensions.

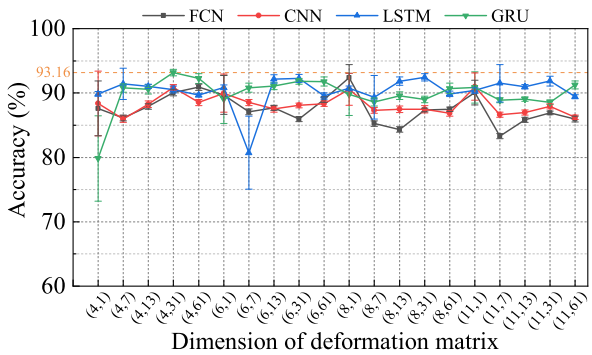

Fig. 11. Accuracy of the trained networks in terms of quantitatively measuring material masses.

of 90.99 ±2.11% at $(11, 1)$. The LSTM network achieves its best accuracy of 91.85±0.77% at $(11, 31)$. The GRU achieves its best accuracy of 93.16±0.50% at $(4, 31)$. Comparatively, the proposed GRU-based weighing method not only achieves the highest accuracy but also has the smallest standard deviation and requires the fewest cross-sections m of the deformation matrix, which is consistent with the network training results.

C. Real-Time Performance Tests

In this part, the performance of the trained networks is tested in a real-time operating system, with a focus on computational speed. Two threads are employed to visually detect the belt contour to perform 3-D reconstruction and mass estimation with the trained network. These tests are executed on an Intel i9 12700 K processor within a Python programming environment. The results are depicted in Fig. 12. The runtime for image processing is approximately 11 ms per frame. The average runtime for the GRU is 51.53 ms, which is shorter than those of the other three

Authorized licensed use limited to: TU Delft Library. Downloaded on January 27,2025 at 09:33:04 UTC from IEEE Xplore. Restrictions apply.

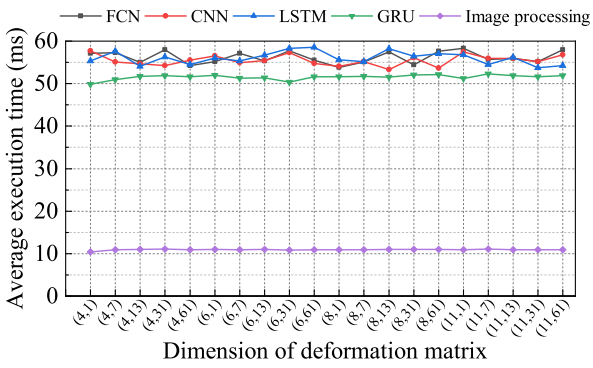

Fig. 12. Average processing time required for image processing and deep learning prediction.

networks (56.21 ms for the FCN, 55.48 ms for the CNN, and 56.04 ms for the LSTM network).

Using dimension $(4, 31)$ as an example, the average prediction time for the GRU-based model is 51.86 ms. Given that the corresponding length of the conveyor belt for the deformation matrix is 240 mm, real-time measurement is achieved at a maximum belt speed of 4.62 m/s.

D. Discussion

The experimental results underscore the potential and feasibility of using DL models to weigh a loaded belt through belt deformation data. In this method, the selection of the dimensions of the deformation matrix is pivotal for ensuring reliable network training and high measurement accuracy. The use of a deformation matrix with too few dimensions risks model underfitting, whereas an overabundance of dimension may diminish the generalizability of the model. At appropriate dimensions of $(4, 31)$, the proposed GRU-based weighing method outperforms other methods in terms of training performance, detection accuracy, and real-time capability.

The complexity of the GRU-based model stems primarily from the GRU layer, which is designed to handle the temporal dependencies in the conveyor belt deformation data. The fully connected layer adds minimal complexity but is crucial for mapping the learned features to the material mass. The dynamicity of the model is well addressed by the ability of the GRU layer to capture long-term dependencies and adapt to real-time data changes. In addition, the model's architecture and training mechanisms ensure that it can be updated to maintain performance in dynamic environments.

This study identifies three primary factors that may constrain the accuracy of the system. First, the current model does not account for the impact of belt tension on deformation, which is a limitation stemming from the absence of tension data in the experimental setup. Belt tension variations associated with the conveyance of different masses can introduce discrepancies during dataset construction and model training, thereby affecting the precision of the model. The integration of tension parameters could unveil a more complex relationship between belt deformation and material mass, hinting at the need for a more sophisticated DL architecture in future research. Second, the reliance of the model on 3-D reconstruction data from image processing implies that any inaccuracies in this step will be propagated to the mass measurement procedure, highlighting the importance of precisely capturing and processing images. Finally, an observed belt deviation of approximately 5 cm in the testing apparatus may have influenced the accuracy of the measurements. Further research is needed to elucidate the extent of the effect of this deviation on the material mass estimates obtained based on belt deformation.

VI. Conclusion

This article presened an innovative visual weighing method for estimating material mass based on belt deformation with a DL algorithm. The method involves detecting the belt deformation field visually, constructing a deformation matrix with specific dimensions, and calculating the material mass via a trained GRU network. By systematic experimentation, suitable dimensions of the deformation matrix are determined, and the proposed weighing method exhibited a better combination of properties than other common DL networks. In this work, we successfully established an accurate model reflecting the inherent correlation between belt deformation and material mass via a GRU network for real-time measurement and achieved intelligent visual perception of material weight. Notably, the proposed method attained an accuracy of 93.16% in experimental testing, highlighting its effectiveness in high-velocity conveyor environments. The proposed method waas compatible with volume flow measurement technologies, facilitating simultaneous mass and volume flow monitoring within a unified system, which indicates its strong potential for industrial adoption.

In future work, we aim to further refine the accuracy of the measurement system. We will investigate the influences of tension fluctuations and belt deviations on the resulting measurement accuracy, to enhance the reliability and applicability of the system in complex industrial environments.

References

[1] L. B. Ristic and B. I. Jeftenic, "Implementation of fuzzy control to improve energy efficiency of variable speed bulk material transportation," *IEEE Trans. Ind. Electron.*, vol. 59, no. 7, pp. 2959–2969, Jul. 2012.

[2] D. He, Y. Pang, and G. Lodewijks, "Green operations of belt conveyors by means of speed control," *Appl. Energy*, vol. 188, pp. 330–341, 2017.

[3] B. Sun, Z. Teng, Q. Hu, S. Tang, W. Qiu, and H. Lin, "A novel LMS-based SANC for conveyor belt-type checkweigher," *IEEE Trans. Instrum. Meas.*, vol. 70, 2021, Art. no. 7500510.

[4] S. Aleksandrovic and J. Mihajlo, "Analysis of belt weigher accuracy limiting factors," *Int. J. Coal Preparation Utilization*, vol. 31, no. 5, pp. 223–241, 2011.

[5] S. Soltani, "The introduction of improved estimation methodology via fuzzy sigma delta for gamma-ray belt conveyor," *IEEE Trans. Ind. Electron.*, vol. 71, no. 6, pp. 6388–6395, Jun. 2024, doi: 10.1109/TIE.2023.3290253.

[6] R. Djokorayono, D. B. Arfittariah Priantama, and T. R. Biyanto, "Design of belt conveyor weight scale using gamma radiation technique," *AIP Conf. Proc.*, vol. 2088, Mar. 2019, Art. no. 020048.

[7] D. Miao, Y. Wang, L. Yang, and S. Wei, "Coal flow detection of belt conveyor based on the two-dimensional laser," *IEEE Access*, vol. 11, pp. 82294–82301, 2023.

[8] F. Zeng, Q. Wu, X. Chu, and Z. Yue, "Measurement of bulk material flow based on laser scanning technology for the energy efficiency improvement of belt conveyors," *Measurement*, vol. 75, pp. 230–243, 2015.

[9] Y. Wang, W. Dai, L. Zhang, and X. Ma, "Coal weight measurement method of belt conveyor based on binocular stereo vision," in *Proc. Int. Conf. Inf., Cybern., Comput. Soc. Syst*, Guangzhou, China, 2020, pp. 486–492.

[10] G. Wang, X. Li, and L. Yang, "Dynamic coal quantity detection and classification of permanent magnet direct drive belt conveyor based on machine vision and deep learning," *Int. J. Pattern Recognit. Artif. Intell.*, vol. 35, no. 11, Art. no. 2152017, 2021.

Authorized licensed use limited to: TU Delft Library. Downloaded on January 27,2025 at 09:33:04 UTC from IEEE Xplore. Restrictions apply.

[11] L. Wen, B. Liang, L. Zhang, B. Hao, and Z. Yang, "Research on coal volume detection and energy-saving optimization intelligent control method of belt conveyor based on laser and binocular visual fusion," *IEEE Access*, vol. 12, pp. 75238–75248, 2024, doi: 10.1109/ACCESS.2023.3261335.
[12] S. Xu, G. Cheng, Z. Cui, Z. Jin, and W. Gu, "Measuring bulk material flow–incorporating RFID and point cloud data processing," *Measurement*, vol. 200, 2022, Art. no. 111598.
[13] J. Yang, C. Wang, B. Jiang, H. Song, and Q. Meng, "Visual perception enabled industry intelligence: State of the art, challenges and prospects," *IEEE Trans. Ind. Inf.*, vol. 17, no. 3, pp. 2204–2219, Mar. 2021.
[14] J. Tian, D. B. Hastie, J. M. Roberts, P. W. Wypych, and R. Pan, "A review of simulation methods for belt conveyors," in *Int. Conf. Bulk Mater. Storage, Handl. Transp.*, Wollongong, Australia, Jul. 2023, pp. 189–200.
[15] D. Ilic and C. Wheeler, "Measurement and simulation of the bulk solid load on a conveyor belt during transportation," *Powder Technol.*, vol. 307, pp. 190–202, 2017.
[16] J. Shen, C. Wheeler, J. OShea, and D. Ilic, "Investigation of the dynamic deflection of conveyor belts via experimental and modelling methods," *Measurement*, vol. 127, pp. 210–220, 2018.
[17] J. Shen, C. Wheeler, D. Ilic, and J. Chen, "Application of open source FEM and DEM simulations for dynamic belt deflection modelling," *Powder Technol.*, vol. 357, pp. 171–185, 2019.
[18] B. Bolat, B. A. Temiztas, E. Sezer, and A. Solak, "Investigation of numerical belt sag and conveyor capacities in inclined belt conveyors: An iterative approach," *Powder Technol.*, vol. 420, 2023, Art. no. 118394.
[19] W. Qiao, Y. Lan, H. Dong, X. Xiong, and T. Qiao, "Dual-field measurement system for real-time material flow on conveyor belt," *Flow Meas. Instrum.*, vol. 83, 2022, Art. no. 102082.
[20] Q. Ni, J. C. Ji, and K. Feng, "Data-driven prognostic scheme for bearings based on a novel health indicator and gated recurrent unit network," *IEEE Trans. Ind. Inf.*, vol. 19, no. 2, pp. 1301–1311, Feb. 2023.
[21] J. Li, C. Yang, Y. Li, and S. Xie, "A context-aware enhanced GRU network with feature-temporal attention for prediction of silicon content in hot metal," *IEEE Trans. Ind. Inf.*, vol. 18, no. 10, pp. 6631–6641, 2022.
[22] F. Zhang, Y. Li, D. Shan, Y. Liu, F. Ma, and W. Yu, "Fault diagnosis algorithm for pumping unit based on dual-branch time-frequency fusion," *IEEE Trans. Rel.*, to be published, doi: 10.1109/TR.2024.3409427.
[23] F. Zhang, K. Sun, and X. Wu, "A novel variable selection algorithm for multi-layer perceptron with elastic net," *Neurocomput.*, vol. 361, pp. 110–118, 2019.
[24] Y. Deng, L. Wang, H. Jia, X. Tong, and F. Li, "A sequence-to-sequence deep learning architecture based on bidirectional GRU for type recognition and time location of combined power quality disturbance," *IEEE Trans. Ind. Inf.*, vol. 15, no. 8, pp. 4481–4493, Aug. 2019.

Wei Qiao received the B.E. degree in mechanical design, manufacturing, and automation from Polytechnic Institute, Taiyuan University of Technology, Taiyuan, China, in 2015, and the M.E. degree in control engineering, in 2018, from Taiyuan University of Technology, where she is currently working toward the Ph.D. degree in mechanical engineering.

Her research interests include machine vision and intelligent measurement.

Xiaoyan Xiong received the Ph.D. degree in mechanical electronics engineering from the Taiyuan University of Technology, Taiyuan, China, in 2008.

She has authored or coauthored more than 100 papers. She also hosts three national natural science projects, one supported program for young provincial academic leaders, and ten provincial-level projects. She is currently a Professor with the Taiyuan University of Technology. Her research interests include mechanical fault diagnosis, modern signal processing, and research on related software and hardware.

Dr. Xiong is the Vice Secretary General of the dynamic testing committee of the Chinese Vibration Engineering Society and is the chairman of the Shanxi Vibration Engineering Society.

Chen Jie received the B.E. degree in software engineering from Shanxi University, Taiyuan, China, in 2018, and the M.E. degree in software engineering from the North University of China, Taiyuan, China, in 2022. He is currently working toward the Ph.D. degree in optical engineering with the Taiyuan University of Technology, Taiyuan, China.

His research interests include photoelectric sensing and intelligent information processing.

Huijie Dong (Member, IEEE) received the B.E. degree in automation from the University of Shanghai for Science and Technology, Shanghai, China, in 2013, and the Ph.D. degree in control theory and control engineering from the Institute of Automation, Chinese Academy of Sciences (IACAS), Beijing, China, in 2022.

He is currently an Assistant Professor with the Key Laboratory of Advanced Transducers and Intelligent Control System, Ministry of Education, Taiyuan University of Technology, Taiyuan, China. His research interests include bioinspired underwater robots and intelligent perception.

Yusong Pang received the M.Sc. degree in electrical engineering from the Taiyuan University of Technology, Taiyuan, China, in 1996 and the Ph.D. degree in intelligent belt conveyor monitoring and control from Delft University of Technology, Delft, The Netherlands, in 2007.

From 2000, he started working with Practic B.V. and Seaview B.V., The Netherlands, for industrial production life cycle management. After his Ph.D. research, he was employed with the Advisory Group Industrial Installations, Royal Haskoning, The Netherlands, in expert material handling. In 2010, he was appointed as Assistant Professor in transport engineering and logistics, Delft University of Technology, The Netherlands. His research interests include the intelligent control for large-scale material handling systems and logistics processes.

Junzhi Yu (Fellow, IEEE) received the B.E. degree in safety engineering and the M.E. degree in precision instruments and mechanology from the North University of China, Taiyuan, China, in 1998 and 2001, respectively, and the Ph.D. degree in control theory and control engineering from the Institute of Automation, Chinese Academy of Sciences, Beijing, China, in 2003.

From 2004 to 2006, he was a Postdoctoral Research Fellow with the Center for Systems and Control, Peking University, Beijing. In 2006, he was an Associate Professor with the Institute of Automation, Chinese Academy of Sciences, where he became a Full Professor in 2012. In 2018, he joined the College of Engineering, Peking University, as a Tenured Full Professor. His current research interests include intelligent robots, motion control, and intelligent mechatronic systems.

Authorized licensed use limited to: TU Delft Library. Downloaded on January 27,2025 at 09:33:04 UTC from IEEE Xplore. Restrictions apply.